Effects of hole transport layer on the performance of sky-blue Dion-Jacobson perovskite light-emitting diodes

Received 00th January 20xx,
Accepted 00th January 20xx

DOI: 10.1039/x0xx00000x

Wen Ting Sun,[a] Yanling He,[a] Muhammad Umair Ali,[a] Qiye Liu,[b] Hongbo Mo,[a] Sijia Wang,[d] Alan Man Ching Ng,[e] and Aleksandra B. Djurišić[a,*]

We investigated the performance of sky-blue quasi-2D Dion-Jacobson perovskite light-emitting diodes as a function of perovskite composition and device architecture. The perovskite composition optimization is needed in order to optimize the film structure to achieve a compromise between efficient funneling and consequent red shift of the emission, and achieving emission in the blue spectral range. Composition optimization was achieved by adjusting the ratio of spacer cations methylenediammonium (MDA) and decanediammonium (DDA) and 3D perovskite $CsPbBr_3$, to achieve films with optimal composition for sky-blue emission. In addition to the perovskite composition, the choice of the hole transport layer (HTL) had a significant effect on the device efficiency. Significant enhancement in the efficiency from 1.8% (control device with self-assembled monolayer HTL) to 4.1% (optimized HTL structure) by inserting diphenyl-4-triphenylsilylphenyl phosphine oxide (TSPO1) between the HTL layers and the perovskite. This results in improved balance of electron and hole injection, as well as passivation of defects in the perovskite, which is responsible for the observed improvements in the device performance.

[a] *Department of Physics, The University of Hong Kong, Pokfulam Road, Hong Kong*
[b] *Shenzhen Institute for Quantum Science and Engineering, and Department of Physics, Southern University of Science and Technology, Shenzhen 518055, China*
[c] *Department of Mechanical Engineering, The University of Hong Kong, Pokfulam Road, Hong Kong*
[d] *Core Characterization Facility, Southern University of Science and Technology, No. 1088, Xueyuan Rd., Shenzhen, 518055, Guangdong, PR China.*
* Corresponding author: Aleksandra B. Djurišić: dalek@hku.hk.
Electronic Supplementary Information (ESI) available: SEM images of the films, SCLC, PL, UPS, TRPL, and device stability plots. See DOI: 10.1039/x0xx00000x

Introduction

Metal halide perovskites hold great potential for light-emitting diode (LED) applications[1-12] due to their exceptional properties, such as tunable emission, high luminescence efficiency, low cost, and simple processes for large-area device fabrication.[1-5] While high external quantum efficiencies (EQE) approaching or even exceeding 25% have been achieved for perovskite LEDs (PeLEDs) in green and red spectral regions,[8,10,11] the efficiency of blue PeLEDs is still lagging behind.[5-9,11,12] In addition, the blue PeLEDs are also commonly suffering from instability issues, such as short lifetime and spectral instability, i.e. shift of the emission wavelength over time.[11-14] Compared to green and red-emitting PeLEDs, perovskite blue emitters have a higher concentration of defects due to their wider bandgap, which also results in unfavorable energy level alignment in devices for efficient carrier injection.[11] The unbalanced charge injection, combined with a higher concentration of nonradiative defects, leads to low efficiency, charge accumulation, and short device lifetime in blue PeLEDs.[11] In addition, the use of mixed Br/Cl halides can lead to phase separation during operation and a red shift of the emission wavelength.[11] These problems inherent to blue perovskite emitters make it challenging to improve the performance of blue LEDs to match the developments in green and red spectral regions. Thus, it is of significant interest to investigate not only the novel perovskite blue emitters but also device architecture to improve the performance of blue PeLEDs.

A possible strategy to address the common problems of perovskite blue emitters is to use quasi-2D halide perovskite materials.[14] These materials are promising for light-emitting applications due to their larger exciton binding energies, and they exhibit improved ambient stability compared to more commonly used 3D perovskites due to increased hydrophobicity owing to the presence of large organic spacer cations,[15-18] as well as reduced ion migration.[15] These materials have a formula $C_xA_{n-1}B_nX_{3n+1}$, where C is the spacer cation, x=1 for diammonium and x=2 for monoammonium spacers, A is the small organic cation or Cs^+, B is divalent metal cation (commonly Pb^{2+} or Sn^{2+}), X is halide anion, while *n* is the number of perovskite octahedral layers separated by spacer cations.[1] The use of quasi-2D perovskites thus enables increased tunability of emission properties by optimizing the composition (number of layers),[1,11] which enables improved PeLED spectral stability by avoiding the use of halide mixing to achieve emission in the blue spectral region, which is a common cause of spectral instability due to halide segregation.[19,20]

However, despite the promising properties of 2D/quasi-2D perovskites for a variety of applications including light emission,[21] there are issues which need to be addressed, namely the achievement of the improved control of the phase distribution (as spin-coated films commonly consist of random distribution and orientation of different *n* phases), inefficient energy funneling, imbalance of charge injection, etc.[1,12]

The issue of energy funneling, i.e. energy transfer from wider bandgap phases to lower bandgap phases, is particularly important in PeLEDs emitting in the blue spectral region, since too high content of low *n* (n=1) phase would result in increased carrier confinement and inefficient funneling and consequently low efficiency, while the presence of high *n* phases would result in the redshift of the emission to the green spectral range.[1,12,17] In general, the emission wavelength of a quasi-2D PeLED is typically controlled by adjusting the ratio of bulky spacer cation and small cation, which results in a variation in the distribution of different *n* phases.[5,11,12] However, it is commonly needed to employ additional methods to simultaneously achieve blue emission and efficient funneling, since this requires not only the suppression of the formation of n=1 phase which leads to inefficient funneling, but also the suppression of formation of n>4 phases which would lead to green emission.[12] One of the approaches to optimize crystallization and phase composition of a quasi-2D perovskite film is spacer cation mixing.[1,5,9,17,22] The spacer cation mixing approach has been used in different quasi-2D materials, including those involving monovalent spacer cations,[1,5,17] divalent spacer cations,[22] and the mixture of monovalent and divalent spacer cations.[9,14] Different spacer cations will have different interactions among the spacer cations, which can affect the formation of low *n* phases, in particular undesirable n=1 phase.[11,12] The use of mixed spacer cations is thus a convenient approach to facilitate the growth of intermediate *n* phases ($1 < n \leq 4$) favorable for the achievement of emission in the blue spectral region.[11,12]

The <100>-oriented 2D and quasi-2D perovskite structures using monovalent spacer cations and displaying offset of (1/2,1/2) in *ab*-plane are called Ruddlesden-Popper (RP) perovskites, while those with divalent spacer cations and no displacement in *ab*-plane are called Dion-Jacobson (DJ) perovskites.[23,24] Compared to RP perovskites, DJ perovskites exhibit higher binding energy between the inorganic perovskite octahedral layers and higher dissociation energy,[1,12,24] and consequently result in improved stability of PeLEDs.[1] This can be attributed to the fact that monoammonium cations in RP perovskites interact with perovskite slab only one side (and spacer cations in a bilayer are bound by weak van der Waals forces), while in DJ perovskites diammonium spacer cations are bound to perovskite slabs on both sides.[11,23,24] Expected improved stability makes DJ perovskites particularly interesting for practical applications, but they have been less commonly studied compared to RP perovskites.[22,25-32] Several works in the literature involve combinations of monovalent and divalent bulky cations,[9,31] or the use of diammonium cations for passivation,[26] while the reports on pure DJ phase perovskites using only divalent spacer cations remain scarce.[22,27-30,32] The scarcity of reports on DJ perovskite PeLEDs could partly occur due to differences in the formation enthalpies for quasi-2D RP and DJ perovskites.[24] It was reported that DJ perovskites exhibit positive formation enthalpies, which makes them metastable.[24] Thus, while this class of materials commonly leads to improved stability in devices,[24] the synthesis of high quality DJ films is likely more difficult compared to RP materials, in particular for blue emitters where both RP and DJ perovskites exhibit difficulty in achieving optimal phase composition for blue emission.

Since DJ perovskites are highly promising, it is of interest to carefully optimize the film composition to achieve blue emission from a DJ perovskite emitter for PeLED applications. As the spacer cation mixing enables improved optimization of phase composition,[1,5,9,12,17,22] we explored the use of mixed diammonium spacer cations, short-chain methylenediammonium (MDA) and long-chain decanediammonium (DDA) to achieve sky-blue emission. The choice of short chain cations, such as MDA, and long chain cations, such as DDA, enables tuning of the phase composition by suppressing the formation of undesirable low *n* (n=1) and high *n* (n>4) phases.[12] MDA was selected since similar monovalent small spacer cation was shown to inhibit the formation of n=1 and high *n* value phases, and thus regulate the confinement and suppress nonradiative recombination when used in combination with bulky cations phenethylammonium (PEA) and butylammonium (BA).[33] DDA was selected as a spacer cation which was reported to result in improved crystallization and efficient green emission in DJ perovskite-based LED.[22]

It should also be noted that the PeLED device performance is significantly affected not only by the perovskite emitter layer, but also by the choice of charge transport layers (CTLs), namely hole transport layer (HTL) and electron transport layer (ETL).[1] These layers need to have favorable energy band alignment with the perovskite to achieve efficient charge injection, and also have low density of interfacial defects at CTL/perovskite interface.[1] The bottom CTL (HTL

in conventional architecture PeLEDs) is particularly important since it can affect the crystallization of the perovskite,[1] and thus affects the phase distribution and consequently funneling, as well as the defect density within the perovskite. In addition to minimizing interfacial defects, it is also necessary to achieve balanced charge injection, since charge injection imbalance not only leads to lower EQE, but also results in charge accumulation which exacerbates degradation and reduces stability.[1] However, achieving balanced charge injection is particularly challenging for blue emitting materials due to their wider bandgap and consequently deeper valence band maximum (VBM) and higher conduction band minimum (CBM).[34] The issues exist for both holes and electrons, since the highest occupied molecular orbital (HOMO) of HTL is commonly higher than the VBM of blue-emitting perovskite, resulting in hole injection barrier.[34] On the other hand, significant differences in electron and hole mobilities in ETL and HTL also result in imbalance of charge injection into the perovskite layer.[34] For example, the most commonly used ETL 2,2',2''-(1,3,5-Benzinetriyl)-tris(1-phenyl-1-H-benzimidazole), TPBi, has significantly lower electron mobility (of the order of 10^{-5} cm^2/Vs) compared to typical values of hole mobility for many different HTLs.[35,36] The imbalanced charge injection due to inferior electron transport then leads to overlap of the emission zone (close to perovskite-ETL interface) and accumulation zone of majority carriers, resulting in low efficiency.[36] This problem could be addressed by design of novel ETLs,[35] or by insertion of interfacial layer to modulate the carrier transport/injection into the perovskite.[36,37] For example, it has been shown that an insertion of hole-blocking cesium acetate layer has significantly increased the efficiency of a blue PeLED.[36] Therefore, here we investigated the effect of the HTL on the performance of DJ DDA-MDA sky-blue PeLEDs. We have considered commonly used hole transport/hole injection materials, such as 2-(9H-carbazol-9-yl)ethyl]phosphonic acid (2PACz)[38] and poly(vinyl carbazole (PVK).[39] Diphenyl-4-triphenylsilylphenyl phosphine oxide (TSPO1)[40] was considered as an interlayer, since this material can passivate the defects in the perovskite,[40] and as an electron transport material[41] it can also be expected to act as a hole blocking material to facilitate more balanced charge injection. We have shown that the insertion of TSPO1 between HTL and perovskite leads to significant improvement in the EQE, which can be attributed to a combined effect of interfacial defect passivation and improvement in charge balance in the devices.

Results and Discussion

The quasi-2D perovskites were obtained by spin-coating a mixture of different ratios of organic diammonium bromide precursor ($DDABr_2$, $MDABr_2$) and $CsPbBr_3$ precursor solutions. We have first investigated the properties of the perovskite with different percentages of $DDABr_2$, as shown in **Figure 1a**. As the $DDABr_2$ ratio increases, a blue shift of the emission as well as the reduction in intensity occurs, and finally multiple peaks appear, consistent with the decreased efficiency of funneling.[42] To achieve blue emission, it is necessary to completely eliminate 3D phase which leads to green emission, while too high content of *n*=1 phase would result in inefficient funneling and hence weak multipeak emission.[12,42] Thus, as a compromise between the two processes, we fixed the ratio of $DDABr_2$ to 45%, and we investigated the effect of the addition of $MDABr_2$, as presented in **Figure 1b** showing normalized PL spectra (PL spectra without normalization are shown in Figure S1) and **Figure 1c**, showing the corresponding absorption spectra. We can observe that the addition of a small amount of $MDABr_2$ induces more formation of the n=2 phase as evidenced by the enhanced exciton absorption peak around 430 nm (**Figure 1c**)). When the content of $MDABr_2$ is at or below 10%, the PL spectra demonstrate comparable emissions with the peak positions in the range of 488-492 nm. With further increase of $MDABr_2$ concentration, the peak broadens and blue shifts, and shoulders appear in the curves, consistent with increased emission from low *n* phases. Thus, DDA-MDA perovskite (45% of $DDABr_2$ and 10% of $MDABr_2$) was utilized as the emissive layer for the fabrication of sky-blue PeLEDs with a structure glass/ITO/HTL/DDA-MDA perovskite/TPBi/Liq/Al, as shown in **Figure 2a**, while SEM image of the device cross-section is shown in **Figure 2b**. The obtained results for 2PACz, 2PACz/PVK, and 2PACz/PVK/TSPO1 HTLs are shown in **Figure 2c-f** and summarized in **Table 1**.

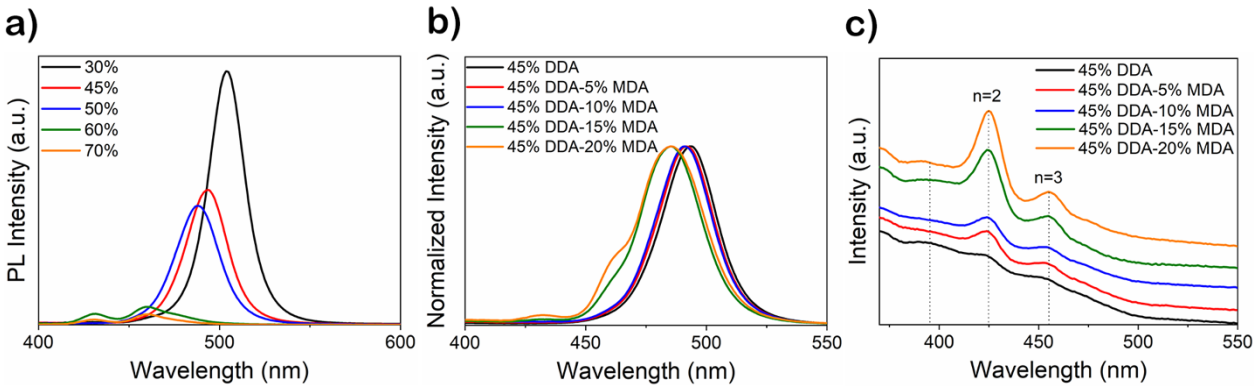

Figure 1. a) PL spectra of perovskites with different content of $DDABr_2$ b) Normalized PL spectra of perovskites with 45% $DDABr_2$ and different content of $MDABr_2$ and c) absorption spectra of DDA-based perovskites with different $MDABr_2$ content.

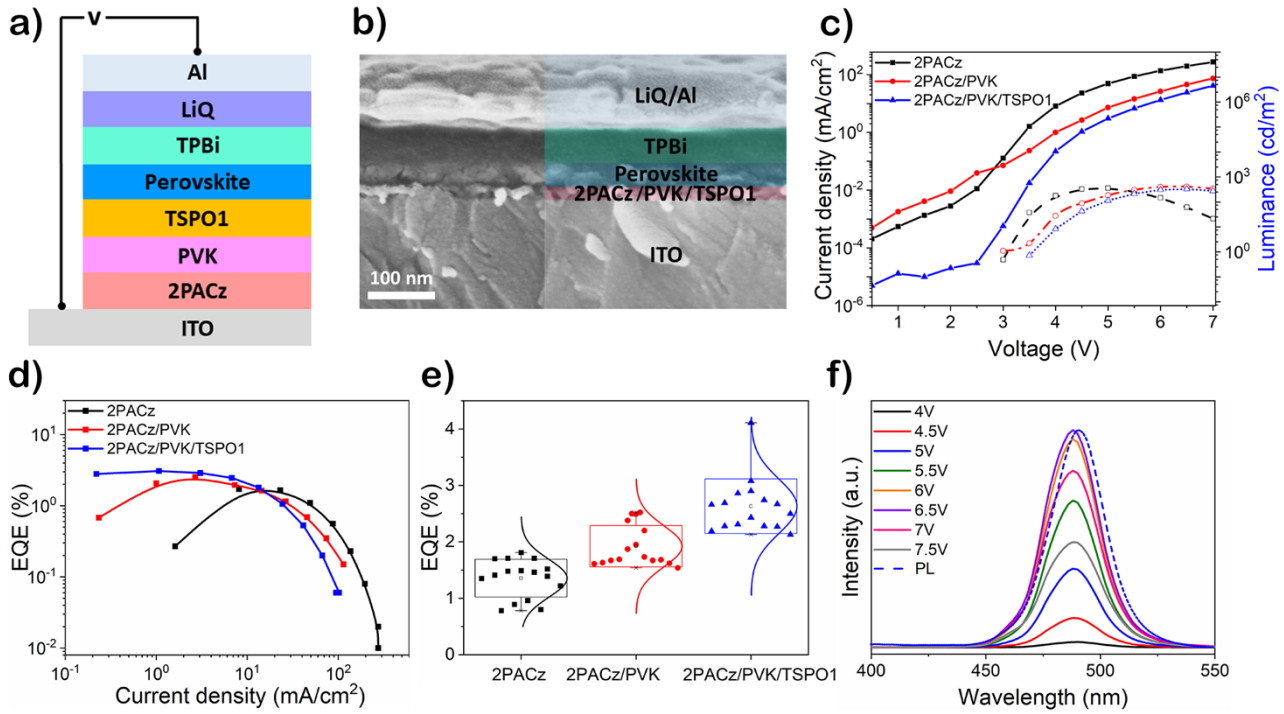

Figure 2. a) Schematic diagram of PeLED, b) cross-section SEM image of PeLED device structure, c) J–V–L curves, d) EQE-J curves, e) EQE histogram, of DDA-MDA perovskite-based LED devices with different HTLs, f) EL spectra of PeLED with TSPO1 layer. PL spectrum is also shown for comparison.

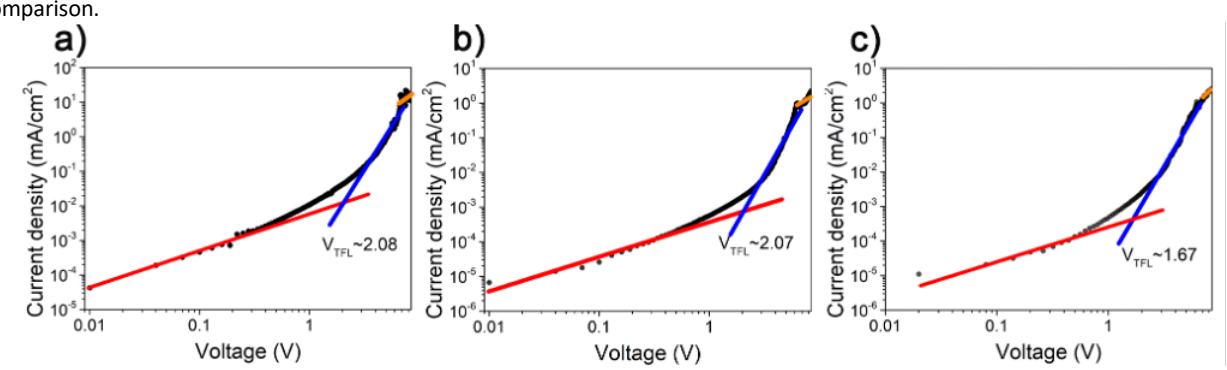

Figure 3. Space-charge-limited current (SCLC) measurement of DDA-MDA perovskite-based LED devices with different HTLs: a) 2PACz, b) 2PACz/PVK, and c) 2PACz/PVK/TSPO1. Device architecture was ITO/HTL/Perovskite/CBP/MoO_x/Al, where CBP denotes 4,4′-bis(N-carbazolyl)-1,1′-biphenyl.

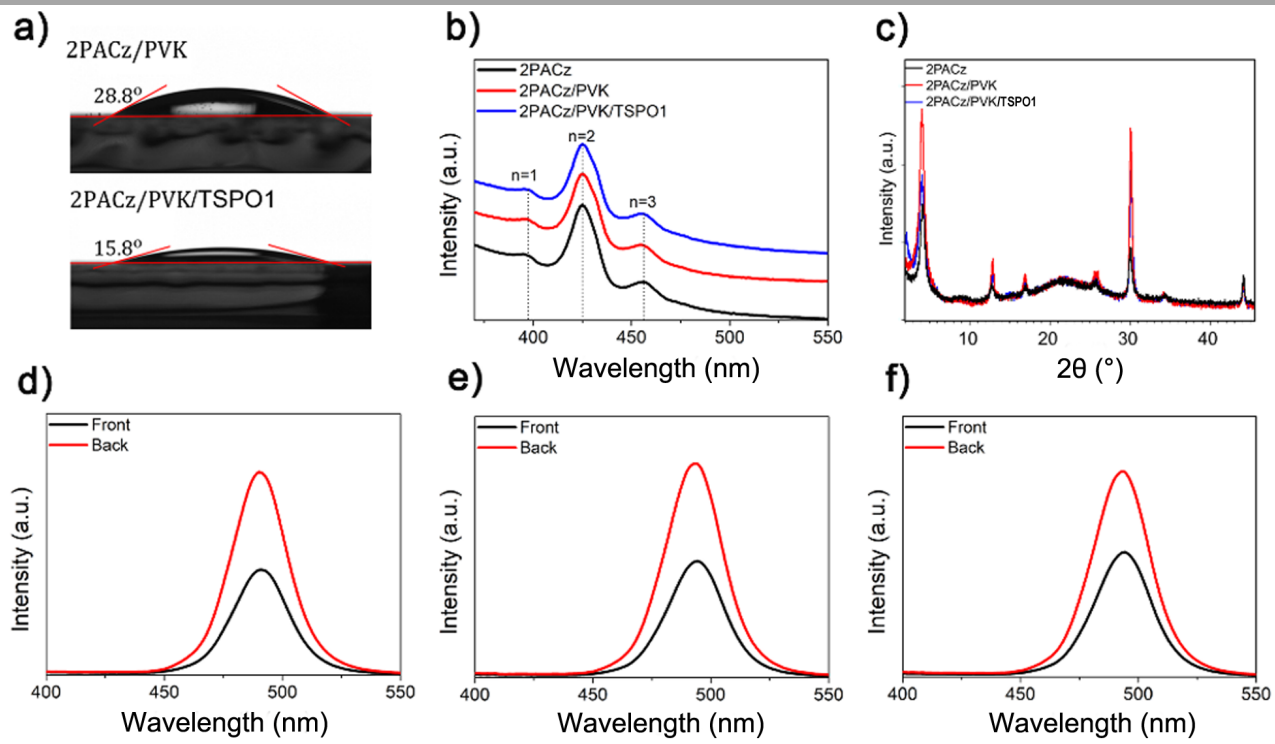

Figure 4. a) Contact angle of DMSO droplet on the PVK and PVK/TSPO1 surface in ambient air, b) absorption spectra, c) XRD pattern, d)-f) PL spectra of DDA-MDA perovskite on different HTLs measured from different sides.

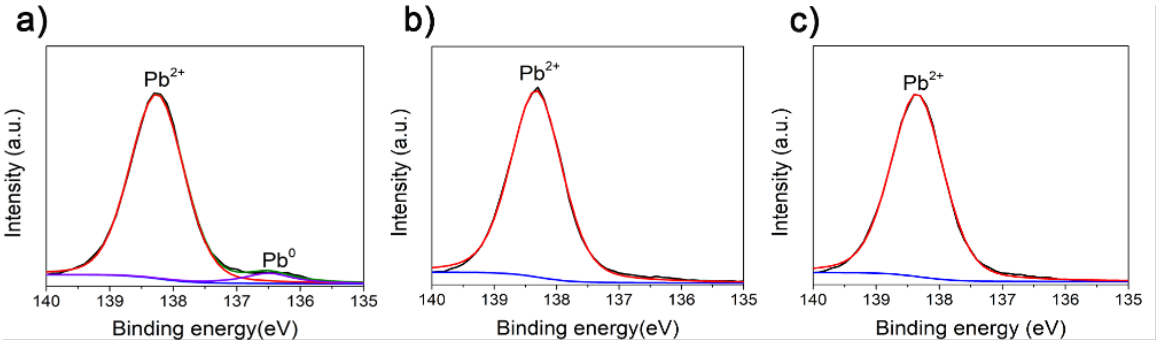

Figure 5. XPS spectra of Pb 4f for perovskite films on a) 2PACz, b)2PACz/PVK, and c) 2PACz/PVK/TSPO1.

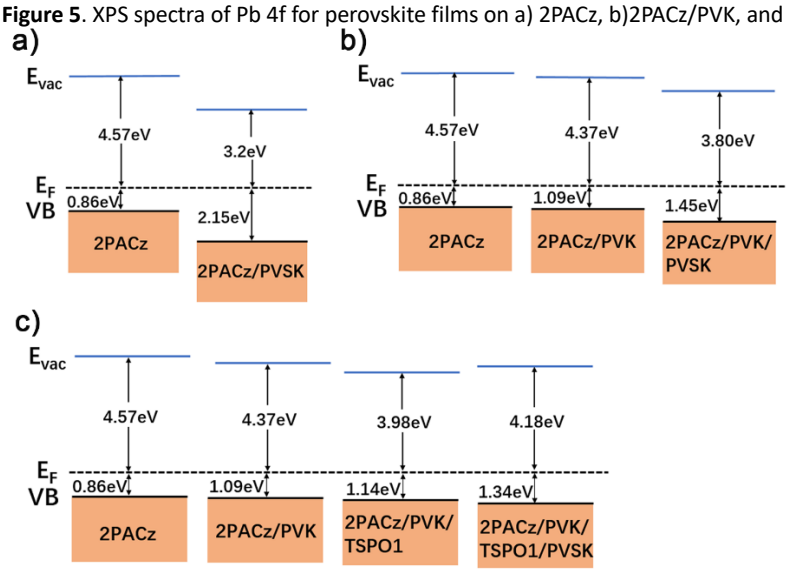

Figure 6. Energy level alignment for different HTLs obtained from UPS measurements and plotted with common Fermi level. PVSK denotes perovskite film.

We can observe that the 2PACz-only device exhibits the lowest EQE of 1.8% with an average value of 1.4%. After lighting up around 3.5V, the luminance rapidly increases to over 300 cd/m^2, followed by a quick decrease, indicating a fast carrier injection into perovskite. Since defects can be observed in perovskite films on 2PACz, as shown in SEM images in **Figure S2**, significant leakage currents are expected. In addition, the fast EQE roll-off (**Figure 2d**) implies the increased non-radiative recombination and unbalanced charge injection,[43] which likely accounts for the low efficiency. The device with PVK layer results in higher maximum brightness (483 cd/m^2) and higher maximum EQE (2.5%). This is at least in part due to improved film morphology, as shown in **Figure S2**. Finally, with TSPO1 we observe further improvement in the efficiency (maximum EQE of 4.1%).

Table 1. Performance parameters of LEDs with different HTLs.

HTL	Avg. Lumin. (cd/m^2)	Max Lumin (cd/m^2)	Avg. EQE (%)	Best EQE (%)	Number of devices
2PACz	304± 54	373	1.4±0.3	1.8	16
2PACz/PVK	354±64	483	1.9±0.4	2.5	16
2PACz/PVK/TSPO1	339±44	391	2.6±0.5	4.1	16

To further investigate reasons for the observed device performance improvements, we have conducted I-V curve measurements for hole-only devices, as shown in **Figure 3**, and electron-only devices, as shown in **Figure S3**. As the electron mobility of TPBi is several orders of magnitude lower compared to hole mobility in common HTL materials,[35,36] we expect the carrier injection to be imbalanced[35] leading to hole accumulation in the devices and unfavorable position of the recombination zone close to perovskite/ETL interface where hole accumulation occurs.[36] We can indeed observe that the current in electron-only devices is lower than that in hole-only devices. In addition, the highest current in hole-only devices is observed for 2PACz devices. The current decreased with the insertion of PVK and TSPO1, consistent with the assumption of improved balance of hole and electron currents. The devices with TSPO1 not only exhibit the lowest current density for hole-only devices and the highest EQE, they also exhibit excellent EL spectral stability with an increasing bias from 4V to over 7V, as shown in Figure 2 f). In addition to improved charge balance, another possible reason for improved performance is defect passivation. Thus, to examine reasons for the observed differences, we have investigated trap densities by space-charge-limited current (SCLC) measurement and photoluminescence quantum yield measurement (PLQY), and we have investigated energy level alignment using ultraviolet photoelectron spectroscopy (UPS) measurements.

The trap density of electrically active defects is commonly estimated from SCLC measurements. The trap-filled limit voltage, V_{TFL}, is commonly determined from the intersection of lines obtained by fitting the Ohmic region and trap-filled limited (TFL) region. The trap density N_t can then be calculated according to the following equation:[44,45]

$$V_{TFL} = \frac{eN_tL^2}{2\varepsilon_0\varepsilon_r}, \qquad (1)$$

where e denotes the unit charge, ε_0 denotes the dielectric constant of vacuum. The relative permittivity ε_r and the thickness L of DDA-MDA perovskites film were 20.72 and 30 nm, respectively. While SCLC is commonly used for determination of trap density in the halide perovskite devices, there are some inherent assumptions made in the model which affect the accuracy and applicability of this analysis.[45] As the ion migration can affect the measurement and the single carrier devices do not consist of a single semiconductor between two ohmic contacts which is assumed in deriving the equations,[45] it is likely that the accuracy of the absolute value of calculated trap density is affected. Nevertheless, relative comparisons between different samples can still provide useful information on possible trap passivation. The calculated trap densities (using transition between Ohmic and TFL regime) of 2PACz-only and 2PACz/PVK devices are 5.3×10^{18} cm^{-3}, slightly higher than that of the device with the TSPO1 layer (4.3×10^{18} cm^{-3}). From the transition point between TFL and Child's law regime (i.e., high injection condition), which has been argued to provide a better estimate,[45] we can obtain trap densities for 2PACz only, 2PACz/PVK, and 2PACz/PVK/TSPO1 of 2.0×10^{19} cm^{-3}, 1.9×10^{19} cm^{-3}, and 1.70×10^{19} cm^{-3}, respectively. Corresponding plots are shown in **Figure S4**. Thus, we can observe the same trends between the values, indicating that any injection difference between the samples is not the likely cause for observed reduction in determined trap density. To obtain an estimate of any difference in the nonradiative defects in the samples, PLQY was measured. The obtained values are 2.4% for 2PACz, 2.6% for 2PACz/PVK, and 3.3% for 2PACz/PVK/TSPO1, confirming the passivation of nonradiative defects by TSPO1. It should be noted that the measured PLQY values are likely underestimated due to transport of samples from Hong Kong to Shenzhen for measurement, which in a very humid climate often results in some deterioration of optical properties even with careful packaging. In addition, PLQY measured from thin films can deviate from expectations due to differences in light extraction from bare perovskite thin films and device architectures. In addition, time resolved photoluminescence (TRPL) measurements have been performed, as shown in **Figure S5** and **Table S1**. TRPL decay curves are commonly fitted with single or biexponential decay, but the interpretation of TRPL decay curves is complex due to multiple contributing processes.[46-48] This is in particular applicable to perovskite films on charge transport layers where charge extraction and non-radiative interface recombination are both present and difficult to disentangle.[46] In addition, passivation induced increase in decay time can be in competition with charge extraction.[48] Considering these facts[46,48] and controversies in attribution of meaning to decay times and calculating average decay time,[47] TRPL results should not be interpreted in isolation. Nevertheless, clear increase in decay time for TSPO1 sample, combined with SCLC results and increase in PLQY can be interpreted as evidence for defect passivation.

Thus, the obtained results indicate that TSPO1 can passivate the perovskite defects, consistent with the presence of P=O which has strong interaction with the Pb.[40] While P=O is also present in the 2PACz molecule, the phosphonic acid part of the self-assembled monolayer (SAM) binds to the oxide surface,[49,50] and thus cannot passivate the defects in the perovskite. To further clarify the role of TSPO1, additional characterization was performed. We can observe that contact angle of DMSO on PVK is reduced from 28.8^o to 15.8^o for PVK/TSPO1, as shown in **Figure 4a**. However, the improved wetting of the perovskite solution only results in a small change in film morphology (**Figure S2b** and **2c**). For all three HTL structures investigated, no change is observed in the absorption spectra of the films, with distinct excitonic features at 423 nm and 460 nm corresponding to n=2 and n=3 phases, respectively. A small shoulder at 390 nm corresponds to the pure 2D structure (n=1). From XRD patterns (**Figure 4c**), there is no significant difference between samples on all three HTLs in terms of the diffraction lines present. We can observe that the sample on 2PACz/PVK exhibits a small improvement in crystallinity, with increased intensity in all diffraction lines. The sample on 2PACz only exhibits the lowest intensity of the diffraction peaks. The ratio of PL intensities (**Figure 4d-f**) measured from the front (perovskite surface) or the back (glass substrate) is 0.52 for the

perovskite film on 2PACz, 0.54 for the film on 2PACz/PVK, and 0.61 for perovskite film on 2PACz/PVK/TSPO1, confirming that TSPO1 affects the native defects in the perovskite. However, no significant differences are observed in device lifetime (**Figure S6**) except for shorter lifetime of devices on 2PACz, indicating that likely different defects affect the ion migration (and thus the lifetime) and nonradiative recombination (and thus the efficiency).

To obtain further insight into the samples, X-ray photoelectron spectroscopy (XPS) measurements were also performed, and the obtained results are shown in **Figure 5**. We can observe the presence of Pb^0 in the perovskite film on 2PACz, in agreement with previous observation of the presence of metallic lead at the interface with 2PACz.[38] This could possibly occur due to weaker binding and lower coverage of phosphonic acid-based SAMs on indium tin oxide (ITO) compared to other oxides, and imperfections in the self-assembly resulting in bare oxide surface.[49,50] Finally, we also performed UPS measurements to establish the effect of HTL structure used on the energy level alignment. It is known that the energy level alignment in perovskite materials is dependent on the dipole moment of the spacer used,[51] and that energy level alignment at interfaces containing organic molecules can be significantly affected by the presence of dipoles resulting in the shift of the vacuum level.[52-54] In addition, the interface dipoles can affect the charge injection.[55-57] Due to alignment of permanent dipole moments of the organic molecules, macroscopic polarization due to spontaneous orientation polarization (SOP) occurs at interfaces, resulting in interface charge and thus electric field.[55,56] The charge accumulation in the devices[56] and the position of the recombination region[55] are thus affected not only by charge injection but also by the presence of SOP.[56] SOP can result in improved charge injection as well as the charge blocking, and the charge carrier balance factor correlates with the interface charge density.[56] When an increased balance of electron and hole currents occurs due to hole blocking caused by interfacial dipole, increased emission efficiency can be obtained.[57] **Figure 6** shows the energy level alignment derived from UPS measurement and plotted with the common Fermi level, while the measured UPS spectra are shown in **Figure S7**. The direction of the vacuum level shift (upward or downward) is dependent on the orientation of the dipoles in the organic molecules,[53,54] with the upward shift occurring when the negative end of the dipole points towards ITO and downward shift occurring when positive end of the dipole points toward the ITO.[54] We can observe that with each consecutive layer, downward shift of the vacuum level occurs, with the only exception being ITO/2PACz/PVK/TSPO1/perovskite structure, where upward shift of the vacuum level indicates the presence of the dipole with positive end pointing towards ITO. Since we also observe a significant decrease in the current in hole-only devices when TSPO1 is inserted between HTL and perovskite (**Figure 2c**), it is likely that the interface dipole due to TSPO1 results in hole blocking and reduced hole injection. Consequently, improved charge injection balance and improved efficiency are obtained when TSPO1 is inserted between PVK and perovskite.

Conclusions

We investigated the effect of perovskite composition and device architecture on the performance of sky-blue PeLEDs with DJ quasi-2D perovskite emitting layers. Optimized perovskite composition resulted in sky-blue emission regardless of the device architecture, but the device efficiency was significantly affected by the HTL selection. Significant improvement in the efficiency was obtained when TSPO1 layer was inserted between the polymer HTL and perovskite, due to the passivation of interfacial defects and the reduction in the hole injection, which lead to more balanced electron and hole currents and consequently higher emission efficiency (best EQE of 4.1 % for devices with TSPO1).

Experimental methods

Materials. Lead bromide ($PbBr_2$, >98%) was purchased from TCI. Cesium bromide (CsBr, 99.9%), tin chloride dihydrate ($SnCl_2{\cdot}2H_2O$, 99.995%), polyethylenimine ethoxylated (PEIE, 37wt.% in H_2O), and chlorobenzene (CB, 99.8%, anhydrous) were purchased from Sigma-Aldrich. Methylenediamine dihydrobromide ($MDABr_2$) decanediamine dihydrobromide ($DDABr_2$), and CBP were purchased from Xi'an Polymer. Dimethyl sulfoxide (DMSO, anhydrous) and isopropyl alcohol (IPA, anhydrous, >99.5+%) were purchased from Alfa Aesar. diphenyl-4-triphenylsilylphenyl phosphine oxide (TSPO1, >99%), 1,3,5-tris(1-phenyl-1H-benzimidazol-2-yl)benzene (TPBi, > 99.8%), and 8-hydroxyquinolinolato-lithium (Liq, >99.9%) were obtained from Luminescence Technology Corporation. Molybdenum oxide (MoO_x) and aluminum pellets (Al) were purchased from Kurt J. Lesker Company. All chemicals were used as received without any purification.

Perovskite film preparation. $PbBr_2$ and CsBr (ratio of 1:1), and $DDABr_2$, and $MDABr_2$ were separately dissolved in DMSO to form the stock solutions of 3D perovskite $CsPbBr_3$ and organic spacers, respectively. The perovskite precursor solutions were obtained by mixing the 3D stock solution with the spacer solutions with a fixed Pb^{2+} concentration of 0.15M. Then the precursor solutions were spin-coated at 4000 rpm for 90 s on different HTLs or well-cleaned quartz substrates, followed by annealing at 95°C for 10 minutes.

Perovskite film characterization: The absorption spectra were obtained by Agilent Cary 60 UV-Vis spectrophotometer. Photoluminescence spectra were collected by a fiberoptic spectrometer and the films were excited by a laser source of HeCd (325nm). Top view and cross-section SEM images were obtained using a Hitachi Regulus 8230 Scanning Electron Microscope. XRD was performed by Rigaku MiniFlex X-ray Diffractometer using Cu Kα radiation. UPS measurements were carried out under 10^{-7} Pa in an ESCALAB 250xi instrument from Thermo Fisher equipped with He I (hν = 21.22 eV) source from a gas discharge lamp. Au was measured as an energy reference and 5 V bias voltage was applied during sample measurements. The contact angles were measured by dropping a DMSO droplet on the different HTL surfaces in air, and images were collected by a Video-based Optical Contact Angle Meter - Model 100SB (Sindatek Instruments Co., Ltd). The TRPL measurements were conducted in a back-reflection geometry. The fundamental wave was generated from a Ti: Sapphire oscillator with an 80MHz repetition rate and 150 fs pulse width. A wavelength of 380 nm was obtained by optical second harmonic generation (SHG) of the fundamental wave of 760 nm. The laser pulses were focused to a spot of around 3μm on the sample at vertical incidence using a 10X objective lens. The reflected PL signals were collected by the same objective lens and detected by PicoHarp 300 with 4 ps resolution. A long pass filter with a central wavelength of 400 nm was used to block the fundamental wave and a bandpass filter with central wavelength of 485 nm was used to select the PL signal. PLQY measurements were carried out using Edinburgh FLS 1000 with an integrating sphere coupled with the fluorescence system. A wavelength of 316 nm was used as excitation source and the spectra were collected with the step increments of 0.5 nm and integration time of 0.1 s per data point. The PLQY was calculated by integrating the emission spectrum from the range of 450 nm to 550 nm.

Device fabrication and characterization. The ITO substrates were sequentially washed in detergent, deionized water, acetone, and ethanol under

ultra-sonication. After blow drying and O_2 plasma treatment, all substrates were transferred into the glovebox filled with Ar gas. The 2PACz films were prepared by spin-coating solution of 2PACz in IPA (0.75 mg/ml) at 4000 rpm for 30 s. For devices with PVK, a layer of PVK (in CB) was spin-coated on 2PACz at 4000 rpm for 30 s, followed by annealing at 120°C for 20 min. For devices with TSPO1, the TSPO1 solution in IPA (dissolved by heating overnight at 70°C) was spin-coated onto PVK at 4000 rpm for 30 s. The DDA-MDA quasi-2D perovskite films were then deposited as previously described. The devices were completed by the thermal deposition of TPBi, Liq, and Al sequentially with an active area of 0.04 cm^2 defined by the shadow mask.

The hole-only devices were fabricated by spin-coating HTL layers in sequence (2PACz, PVK, TSPO1) on well-cleaned ITO substrate in sequence, followed by spin-coating of perovskite film and thermal deposition of CBP/MoO_x/Al. For the electron-only device, SnO_2 sol-gel solution was prepared by dissolving 45mg $SnCl_2 \cdot 2H_2O$ in 1ml ethanol under heating at 50 °C for 1 h. Then the mixture was spin-coated on ITO substrates at 3000 rpm for 30 s, followed by annealing at 275 °C for 30 min. A thin layer of PEIE and the perovskite film were subsequently deposited on the SnO_2 film, followed by thermal evaporation of TPBi/Liq/Al.

The electroluminescence (EL) spectra and external quantum efficiency (EQE) was characterized by the Keithley 2400 source meter connected with a Photoresearch PR-670 spectroradiometer with SL-1X close-up lens. Device lifetime was determined by measuring luminance over time at a constant current bias of 0.2 mA which corresponded to initial luminance in the range 90-99 cd/m^2. The I-V curves for space-charge-limited-current (SCLC) measurements were measured with the Keithley 2400 source meter.

Author Contributions

A. B. D. designed the whole study, analysed and interpreted results. W. T. S. prepared the samples and performed characterization with assistance from M. U. A., while W. T. S. and A. B. D. wrote the first draft of the manuscript. S. J. W. performed contact angle measurements. Y. H. performed PLQY, UPS and XPS measurements, and provided the analysis together with A. M. C. N. TRPL measurements were performed by Y. H. and Q. L., while the analysis was performed by H. M. All authors contributed to the final version of the text.

Conflicts of interest

There are no conflicts to declare.

Acknowledgements

This work was supported by the NSFC project 6207032617 and RGC GRF project 17301520, RGC CRF project 7035-20G, Seed Funding for Basic Research and Seed Funding for Strategic Interdisciplinary Research Scheme of the University of Hong Kong.

Notes and references

‡ Footnotes relating to the main text should appear here. These might include

1 Yukta, S. Satapathi, Strategies to Enhance Light Emission from Two-Dimensional Perovskite Light-Emitting Diodes: Challenges and Future Opportunities, *ACS Appl. Electron. Mater.,* 2022, **4**, 1469-1484
2 L. N. Quan, B. P. Rand, R. H. Friend, S. G. Mhaisalkar, Perovskites for Next-Generation Optical Sources, *Chem. Rev*., 2019, **119**, 7444-7477
3 J. Byun, H. Cho, C. Wolf, M. Jang, A. Sadhanala, R. H. Friend, H. Yang, T. Lee, Efficient Visible Quasi-2D Perovskite Light-Emitting Diodes, *Adv. Mater.,* 2016, **28**, 7515-7520
4 P. Vashishtha, M. Ng, S. B. Shivarudraiah, J. E. Halpert, High Efficiency Blue and Green Light-Emitting Diodes Using Ruddlesden–Popper Inorganic Mixed Halide Perovskites with Butylammonium Interlayers, *Chem. Mater*., 2019, **31**, 83-89
5 M. H. Park, 3D and 2D Metal Halide Perovskites for Blue Light-Emitting Diodes, *Materials* 2022, **15**, 4571.
6 Z. Zhu, Y. Wu, Y. Shen, J. Tan, D. Shen, M. Lo, M. Li, Y. Yuan, J. Tang, W. Zhang, S. Tsang, Z. Guan, C. Lee, Highly Efficient Sky-Blue Perovskite Light-Emitting Diode Via Suppressing Nonradiative Energy Loss, *Chem. Mater.*, 2021, **33**, 4154-4162
7 Z. Liu, W. Qiu, X. Peng, G. Sun, X. Liu, D. Liu, Z. Li, F. He, C. Shen, Q. Gu, F. Ma, H. Yip, L. Hou, Z. Qi, S. Su, Perovskite Light-Emitting Diodes with EQE Exceeding 28% through a Synergetic Dual-Additive Strategy for Defect Passivation and Nanostructure Regulation, *Adv. Mater.,* 2021, **33**, 2103268
8 J. Jiang, Z. Chu, Z. Yin, J. Li, Y. Yang, J. Chen, J. Wu, J. You, X. Zhang, Red Perovskite Light-Emitting Diodes with Efficiency Exceeding 25% Realized by Co-Spacer Cations, *Adv. Mater.,* 2022, **34**, 2204460
9 S. Yuan, Z. Wang, L. Xiao, C. Zhang, S. Yang, B. Chen, H. Ge, Q. Tian, Y. Jin, L. Liao, Optimization of Low-Dimensional Components of Quasi-2D Perovskite Films for Deep-Blue Light-Emitting Diodes, *Adv. Mater.*, 2019, **31**, 1904319
10 H. Wang, W. D. Xu , Q. Wei, S. Peng, Y. Q. Shang, X. Y. Jiang, D. Yu, K. Wang, R. H. Pu, C. X. Zhao, Z. H. Zang, H. S. Li, Y. L. Zhang, T. Pan, Z. J. Peng, X. Q. Shen, S. J. Ling, W. M. Liu, F. Gao, Z. J. Ning, In-situ growth of low-dimensional perovskite- based insular nanocrystals for highly efficient light emitting diodes, *Light Sci. Appl.,* 2023, **12**, 62
11 K. Zhang, L. X. Cao, Y. Y. Tang, Y. Yu, Y. Shen, B. F. Wang, W. J. Wang, Y. Q. Li, J. X. Tang, Blue Halide Perovskite Materials: Preparation, Progress, and Challenges, *Laser Photonics Rev.* 2023, **17**, 2200689
12 G. S. Kumar, R. R. Sumukam, B. Murali, Quasi-2D perovskite emitters: a boon for efficient blue light-emitting diodes, *J. Mater. Chem. C*, 2020, **8**, 14334—14347
13 F. Ye, Q. Shan, H. Zeng, W. C. H. Choy, Operational and Spectral Stability of Perovskite Light-Emitting Diodes, *ACS Energy Lett.,* 2021, **6**, 3114-3131
14 Y. Jiang, C. Qin, M. Cui, T. He, K. Liu, Y. Huang, M. Luo, L Zhang, H. Xu, S. Li, J. Wei, Z. Liu, H. Wang, G. Kim, M. Yuan, J. Chen, Spectra Stable Blue Perovskite Light-Emitting Diodes, *Nat. Commun.,* 2019, **10**, 1868
15 L. Mao, C. C. Stoumpos, M. G. Kanatzidis, Two-Dimensional Hybrid Halide Perovskites: Principles and Promises, *J. Am. Chem. Soc.,* 2019, **141**, 1171-1190
16 C. Katan, N. Mercier, J. Even, Quantum and Dielectric Confinement Effects in Lower-Dimensional Hybrid Perovskite Semiconductors, *Chem. Rev.* 2019, **119**, 5, 3140-3192
17 Y. Xia, Y. Li, Z. Wang, L. Liao, Domain Distribution Management of Quasi-2D Perovskites toward High-Performance Blue Light-Emitting Diodes, *Adv. Funct. Mater.*, 2023, 2303423
18 D. Yang, B. Zhao, T. Yang, R. Lai, D. Lan, R. H. Friend, D. Di, Toward Stable and Efficient Perovskite Light-Emitting Diodes, *Adv. Funct. Mater.*, 2022, **32**, 2109495

19 Y. H. Zhou, Y. H. Lou, X. Q. Wang, K. L. Wang, J. Chen, C. H. Chen, Z. K. Wang, *Adv. Opt. Mater.* 2022, **10**, 2101655.

20 Y. Zhou, C. Wang, S. Yuan, C. Zou, Z. Su, K. Wang, Y. Xia, B. Wang, D. Di, Z. Wang, L. Liao, Stabilized Low-Dimensional Species for Deep-Blue Perovskite Light-Emitting Diodes with EQE Approaching 3.4%, *J. Am. Chem. Soc.*, 2022, **144**, 18470-18478

21 K. Zheng, T. Pullerits, Two Dimensions Are Better for Perovskites, *J. Phys. Chem. Lett.,* 2019, **10**, 5881-5885

22 X. S. Qin, F. Z. Liu, T. L. Leung, W. T. Sun, C. C. S. Chan, K. S. Wong, L. Kanižaj, J. Popović, A. B. Djurišić, „Compositional optimization of mixed cation Dion-Jacobson perovskites for efficient green light emission “, *J. Mater. Chem. C* 2022, **10**, 108 – 114.

23 P. Huang, S. Kazim, M. K. Wang, S. Ahmad, Toward Phase Stability: Dion–Jacobson Layered Perovskite for Solar Cells, *ACS Energy Lett*. 2019, **4**, 2960−2974.

24 I. Metcalf, S. Sidhik, H. Zhang, A. Agrawal, J. Persaud, J. Hou, J. Even, A. D. Mohite, Synergy of 3D and 2D Perovskites for Durable, Efficient Solar Cells and Beyond, *Chem. Rev.* 2023, 10.1021/acs.chemrev.3c00214.

25 N. Zhou, H. Zhou, Spacer Organic Cation Engineering for Quasi-2D Metal Halide Perovskites and the Optoelectronic Application, *Small Struct.,* 2022, **3**, 2100232

26 N. Li, S. Apergi, C. C. S. Chan, Y. Jia, F. Xie, Q. Liang, G. Li, K. S. Wang, G. Brocks, S. Tao, N. Zhao, Diammonium-Mediated Perovskite Film Formation for High-Luminescence Red Perovskite Light-Emitting Diodes, *Adv. Mater.,* 2022, **34**, 2202042

27 Y. Shang, Y. Liao, Q. Wei1, Z. Wang, B. Xiang, Y. Ke,W. Liu, Z. Ning, Highly Stable Hybrid Perovskite Light-Emitting Diodes Based on Dion-Jacobson Structure, *Sci. Adv.*, 2019, **5**, eaaw8072

28 Y. Liu, L. K. Ono, G. Tong, H. Zhang, Y. Qi, Two-Dimensional Dion–Jacobson Structure Perovskites for Efficient Sky-Blue Light-Emitting Diodes, *ACS Energy Lett.,* 2021, **6**, 908-914

29 C. Chen, Z. Li, Q. Xue, Y. Su, C. Lee, H. Yip, W. Chen, C. Chueh, Engineering of Perovskite Light-Emitting Diodes Based on Quasi-2D Perovskites Formed by Diamine Cations, *Org. Electron.,* 2019, **75**, 105400

30 Y. Liu, L. K. Ono, G. Tong, T. Bu, H. Zhang, C. Ding, W. Zhang, Y. Qi, Spectral Stable Blue-Light-Emitting Diodes via Asymmetric Organic Diamine Based Dion−Jacobson Perovskites, *J. Am. Chem. Soc.,* 2021, **143**, 19711−19718

31 X. F. Peng, B. C. He, H. L. Zheng, Z. S. Su, X. Z. Li, L. Ji, T. Zhang, L. Chen, C. C. Qin, X. Y. Gao, S. B. Li, X. H. Yang, Suppressed Energy Transfer Loss of Dion−Jacobson Perovskite Enabled by DMSO Vapor Treatment for Efficient Sky-Blue Light-Emitting Diodes, ACS Energy Lett. 2023, **8**, 339−346

32 H. J. Yang, J. Tang, L. L. Deng, Z. Liu, X. Yang, Z. Q. Huang, H. M. Yu, K. Wang, J. P. Li, Improved highly efficient Dion–Jacobson type perovskite light-emitting diodes by effective surface polarization architecture, *Phys. Chem. Chem. Phys*., 2022, **24**, 7969-7977.

33 S. Zeng, S. Shi, S. Wang, Y. Xiao, Mixed-ligand engineering of quasi-2D perovskites for efficient sky-blue light-emitting diodes, J. Mater. Chem. C, 2020, 8, 1319.

34 X. Qian, Y. Tang, W. Zhou, Y. Shen, M. Guo, Y. Li, J. Tang, Strategies to Improve Luminescence Efficiency and Stability of Blue Perovskite Light-Emitting Devices, *Small Sci.*, 2021, **1**, 2000048

35 Z. Zhu, Y. Li, Z. Guan, Y. Wu, Z. Zeng, S. Tsang, S. Liu, X. Huang, C. Lee, Spatial Control of the Hole Accumulation Zone for Hole-Dominated Perovskite Light-Emitting Diodes by Inserting a CsAc Layer, *ACS Appl. Mater. Interfaces*, 2023, **15**, 7044-7052

36 S. Yuan, T. Fang, J. Huang, X. Li, C. Wei, Y. Zhou, Y. Li, X. Zheng, J. Huang, J. Su, G. Baryshnikov, W. C. H. Choy, H. Zeng, B. Xu, Balancing Charge Injection via a Tailor-Made Electron-Transporting Material for High Performance Blue Perovskite QLEDs, *ACS Energy Lett.,* 2023, **8**, 818-826

37 T. Han, S. Tan, J. Xue, L. Meng, J. Lee, Y. Yan, Interface and Defect Engineering for Metal Halide Perovskite Optoelectronic Devices, *Adv. Mater.*, 2019, **31**, 1803515

38 W. T. Xiong, C. Zou, W. D. Tang, S. Y. Xing, Z. Y. Wang, B. D. Zhao, D. W. Di, Efficient and Bright Blue Perovskite LEDs Enabled by a Carbazole-Phosphonic Acid Interface, *ACS Energy Lett.* 2023, **8**, 2897−2903

39 L. J. Yang, Y. Yan, F. Cai, J. Li, T. Wang, Poly(9-Vinylcarbazole) as a Hole Transport Material for Efficient and Stable Inverted Planar Heterojunction Perovskite Solar Cells, *Sol. Energy Mater. Sol. Cells,* 2017, **163**, 210-217

40 L. Xu, J. Li, B. Cai, J. Song, F. Zhang, T. Fang, H. Zeng, A Bilateral Interfacial Passivation Strategy Promoting Efficiency and Stability of Perovskite Quantum Dot Light-Emitting Diodes, *Nat. Commun.*, 2020, **11,** 3902.

41 Z. Chen, N. T. Tian, P. Tao, S. M. Chen, D. G. Ma, L. X. Wang, W. Y. Wong, A Pure Blue Phosphorescent Organic Light-Emitting Diode with an External Quantum Efficiency of Over 30% by Using a Tandem Device Architecture, *Adv. Mater. Interfaces* 2022, **9**, 2200932.

42 N. Yantara, N. F. Jamaludin, B. Febriansyah, D. Giovanni, A. Bruno, C. Soci, T. C. Sum, S. Mhaisalkar, N. Mathews, Designing the Perovskite Structural Landscape for Efficient Blue Emission, *ACS Energy Lett.* 2020, **5**, 1593−1600.

43 A. Fakharuddin, M. K. Gangishetty, M. Abdi-Jalebi, S. Chin, Abd. Rashid bin Mohd Yusoff, D. N. Congreve, W. Tress, F. Deschler, M. Vasilopoulou, H. J. Bolink, Perovskite Light-Emitting Diodes, *Nat. Electron.,* 2022, **5**, 203-216

44 V. M. L. Corre, E. A. Duijnstee, O. E. Tambouli, J. M. Ball, H. J. Snaith, J. Lim, L. J. A. Koste, Revealing Charge Carrier Mobility and Defect Densities in Metal Halide Perovskites via Space-Charge-Limited Current Measurements, *ACS Energy Lett.*, 2021, **6**, 1087-1094.

45 C. X. Bao, F. Gao, Physics of defects in metal halide perovskites, Rep. Prog. Phys., 2022, **85**, 096501

46 M. Stolterfoht, C. M. Wolff, J. A. Márquez, S. Zhang, C. J. Hages, D. Rothhardt, S. Albrecht, P. L. Burn, P. Meredith, T. Unold, D. Neher, Visualization and suppression of interfacial recombination for high-efficiency large-area pin perovskite solar cells, *Nat. Energy* 2018, **3**, 847-854.

47 J. Chen, J. Lv, X. Liu, J. Lin, X. Chen, A study on theoretical models for investigating time-resolved photoluminescence in halide perovskites, *Chem Phys Phys Chem* 2023, **25**, 7574-7588.

48 W. Wang, D. Zhang, R. Liu, D. T. Gangadharan, F. Tan, M. I. Saidaminov, Characterization of interfaces: Lessons from the past for the future of perovskite solar cells, *J. Semicond.* 2022, **43**, 051202.

49 N. Phung, M. Verheijen, A. Todinova, K. Datta, M. Verhage, A. Al-Ashouri, H. Köbler, X. Li, A. Abate, S. Albrecht, M. Creatore, Enhanced Self-Assembled Monolayer Surface Coverage by ALD NiO in p-i-n Perovskite Solar Cells, *ACS Appl. Mater. Interfaces* 2022, **14**, 2166-2176.

50 J. J. Sun, C. H. Shou, J. S. Sun, X. L. Wang, Z. H. Yang, Y. Chen, J. R. Wu, W. C. Yang, H. L. Long, Z. Q. Ying, X. Yang, J. Sheng, B. J. Yan, J. C. Ye, NiO_x-Seeded Self-Assembled Monolayers as Highly Hole-Selective Passivating Contacts for Efficient Inverted Perovskite Solar Cells, *Solar RRL* 2021, **5**, 2100663.

51 M. Worku, A. Ben-Akacha, S. Sridhar, J. R. Frick, S. C. Yin, Q. Q. He, A. J. Robb, M. Chaaban, H. Liu, J. S. R. V. Winfred, K. Hanson, F. So, D.Dougherty, B. W.Ma, Band Edge Control of Quasi-2D Metal Halide Perovskites for Blue Light-Emitting Diodes with Enhanced Performance, *Adv. Funct. Mater*. 2021, 31, 2103299.

52 E. Zojer, T. C. Taucher, O. T. Hofmann, The Impact of Dipolar Layers on the Electronic Properties of Organic/Inorganic Hybrid Interfaces, *Adv. Mater. Interfaces* 2019, **6**, 1900581.
53 E. L. Ratcliff, J. Meyer, K. X. Steirer, N. R. Armstrong, D. Olson, A. Kahn, Energy level alignment in PCDTBT:$PC_{70}BM$ solar cells: Solution processed NiO_x for improved hole collection and efficiency, *Org. Electron.* 2012, **13**, 744–749
54 Q. Chen, C. Wang, Y. W. Li, L. W. Chen, Interfacial Dipole in Organic and Perovskite Solar Cells, *J. Am. Chem. Soc*. 2020, **142**, 18281−18292
55 X. T. Xiao, K. Wang, T. K. Ye, R. Cai, Z. W. Ren, D. Wu, X. W. Qu, J. Y. Sun, S. H. Ding, X. W. Sun, W. C. H. Choy, Enhanced hole injection assisted by electric dipoles for efficient perovskite light-emitting diodes, *Commun. Mater.* 2020, **1**, 81.
56 Y. Noguchi, A. Hofmann, W. Brütting, Controlling Charge Accumulation Properties of Organic Light-Emitting Diodes using Dipolar Doping of Hole Transport Layers, *Adv. Opt. Mater.* 2022, **10**, 2201278
57 C. C. Hsiao, C. H. Chang; T. H. Jen; M. C. Hung, S. A. Chen, High-efficiency polymer light-emitting diodes based on poly[2-methoxy-5-(2-ethylhexyloxy)-1,4-phenylene vinylene] with plasma-polymerized -modified indium tin oxide CHF_3 as an anode, *Appl. Phys. Lett.* 2006, **88**, 033512

Table of Contents

Increased efficiency of sky-blue LEDs based on Dion-Jacobson perovskite emitter occurs with optimization of hole transport layer-perovskite interface.